ELSEVIER

Catalysis Today 78 (2003) 529–538

CATALYSIS TODAY

www.elsevier.com/locate/cattod

Dielectric loss and phase transition of sodium potassium niobate ceramic investigated by impedance spectroscopy

M.A.L. Nobre[1], S. Lanfredi*

Instituto de Física de São Carlos, Universidade de São Paulo, C.P. 369, 13560-970, São Carlos, SP, Brazil

Abstract

The dielectric permittivity of $Na_{0.80}K_{0.20}NbO_3$ ceramic was investigated by impedance spectroscopy. The dielectric characterization was performed from room temperature to 800 °C, in the frequency range 5 Hz–13 MHz. The bulk permittivity was derived by the variation of the imaginary part of the impedance as a function of reciprocal angular frequency. The permittivity values as a function of temperature showed two maxima. The first maximum is very similar at 200 °C and the second one positioned at around 400 °C, which was associated to Curie's temperature. The evolution of the complex permittivity as a function of frequency and temperature was investigated. At low frequency dispersion was investigated in terms of dielectric loss. The $Na_{0.80}K_{0.20}NbO_3$ showed a dissipation factor between 5 and 40 over a frequency range from 1 to 10^2 kHz.

Keywords: Dielectric loss; Phase transition; Impedance spectroscopy

1. Introduction

The solid solution $Na_{1-x}K_xNbO_3$ is considered an advanced ferroelectric material for high frequency applications [1]. Studies based on the alkaline niobates as new dielectric materials have been carried out to attain suitable materials for high applications performance, which require a combination of advanced characteristics, such as low dielectric loss, low aging coefficient, high permittivity and planar coupling coefficient [2]. Several investigations of the physical properties of alkaline niobates with perovskites type structure have been reported. As a whole, $NaNbO_3$ is considered as a host structure, which is known to be antiferroelectric, belonging to the orthorhombic system at room temperature. Optical studies and X-ray diffraction of this material have revealed seven phase transitions occurring between −110 and 640 °C [3]. On the other hand, $KNbO_3$ presents only two phase transition between the room temperature and 400 °C [4]. The first one is centered at around 200 °C being associated with an orthorhombic–tetragonal phase transition, while the second one is positioned at around 400 °C. This transition is correlated to the tetragonal–cubic phase transition. This one has been assigned to Curie's temperature [5]. At room temperature, $KNbO_3$ is ferroelectric exhibiting a orthorhombic structure. The permittivity properties of the sodium niobate shows a maximum at 360 °C. At this temperature, a change of symmetry occurs being accompanied of a remarkable evolution of the pseudo-cubic deformation degree [6,7]. This temperature of transition is termed as Curie's temperature, where occurs

* Corresponding author. Present address: Faculdade de Ciências e Tecnologia de Presidente Prudente, Universidade Estadual Paulista, UNESP, C.P. 467, CEP 19060-080, Presidente Prudente, SP, Brazil.
E-mail address: silvania@ifsc.sc.usp.br (S. Lanfredi).
[1] Present address: Faculdade de Ciências e Tecnologia de Presidente Prudente, Universidade Estadual Paulista, UNESP, C.P. 467, CEP 19060-080, Presidente Prudente, SP, Brazil.

0920-5861/02/$ – see front matter
PII: S0920-5861(02)00349-8

a ferroelectric–antiferroelectric or antiferroelectric–paraelectric transition. Despite of $NaNbO_3$ presents ferroelectricity only at temperature under −110 °C, the addition of $KNbO_3$ to $NaNbO_3$, even small amounts, leads to ferroelectricity properties phase development at room temperature [5]. The variations of Curie's temperature of $NaNbO_3$ with the formation of solid solutions due to the addition of $KNbO_3$ indicate that piezoelectric, pyroelectric and eletrooptic applications may be expected. Despite these promising properties, few studies have been reported on the high temperature dielectrical properties of polycrystalline $Na_{1-x}K_xNbO_3$ systems synthesized via a chemical route.

The ac analysis technique has been widely used to investigate the dielectric behavior of amorphous and polycrystalline materials [8,9]. This technique, whether applied to ceramics, allows to separate the electric and dielectric properties of the grain (bulk contribution) from those corresponding to the grain boundaries and their interface with electrodes. This paper reports the newest results from studies on the electric and dielectric properties of dense ceramics of sodium potassium niobate using impedance spectroscopy. The $Na_{0.80}K_{0.20}NbO_3$ solid solution was synthesized by chemical route using the thermal decomposition of the precursor salt, which was prepared by the evaporation solution method [10]. An investigation is presented here for the dielectric behavior of $Na_{0.80}K_{0.20}NbO_3$ solid solution, with controlled stoichiometry, at high temperature.

2. Experimental procedure

2.1. $Na_{0.80}K_{0.20}NbO_3$ synthesis

The precursor of $Na_{0.80}K_{0.20}NbO_3$ was synthesized by a chemical evaporation method [10,11]. Potassium nitrate, sodium nitrate and a soluble niobium complex salt, $NH_4H_2[NbO(C_2O_4)_3]{\cdot}3H_2O$, provided by CBMM (Companhia Brasileira de Metalurgia e Mineração, Araxá-MG—Brazil), were used as starting reagents. A saturated solution of oxalic acid was added to a solution of sodium and potassium nitrate in deionized water, monitored by a digital pH-meter, until the pH to reach a value equal to 1. Then, the pH was adjusted to 3 by addition of a 1:1 ammonium hydroxide solution. After stirring for 10 min, a 0.7 mol^{-1} niobium salt solution was added, leading to a final solution of pH equal to 2. This solution was refluxed for 3 h at 80 °C. After refluxing, the solution was maintained at 70 °C until the point of complete evaporation and formation of the precursor powder. This precursor was triturated in a agate mortar and calcined in air atmosphere at temperatures between 250 and 700 °C. Crystalline and single phase powder of $Na_{0.80}K_{0.20}NbO_3$ was obtained with the calcination of the precursor powder at 700 °C for 5 h. An X-ray powder analysis showed only the diffraction lines of the orthorhombic phase of sodium niobate (JCPDS—Card 33-1270) [12].

2.2. Structural characterization

The thermogravimetry and differential thermal analysis were performed using NETZSCH Simultaneous Thermal Analyser—STA 409 from room temperature to 900 °C under dry air. The heating rate was fixed at 10 °C/min. The X-ray powder diffraction pattern was obtained using Cu Kα radiation (D5000, Kristalloflex-Siemens) in the 2θ range from 5° to 75°.

2.3. Chemical analysis

The chemical analysis of the $Na_{0.80}K_{0.20}NbO_3$ solid solution was carried out by inductively coupled plasma emission spectroscopy with a Thermo-Jarrel-Ash atomscan 25 instrument. The $Na_{0.80}K_{0.20}NbO_3$ obtained by heating of the precursor at 700 °C revealed 55.50 wt.% Nb, 11.15 wt.% Na and 4.49 wt.% K, which corresponds to a Nb/Na mole ratio of 0.81 and the Nb/K mole ratio of 0.19. Theses values are in an excellent agreement with the expected theoretical ones: 55.58 wt.% Nb, 11.01 wt.% Na and 4.66 wt.% K.

2.4. Compaction and sintering procedure

Powder calcined previously was deagglomerated by dry milling in an agate mortar, followed by the addition of 2 wt.% of polyvinyl butiral used as a binder. This mixture was pressed in disk form under a 10 kPa uniaxial pressure followed by a 100 MPa isostatic pressure obtaining pellet with a 1.1 mm thickness and a 12 mm diameter. This pellet was heated at 500 °C for

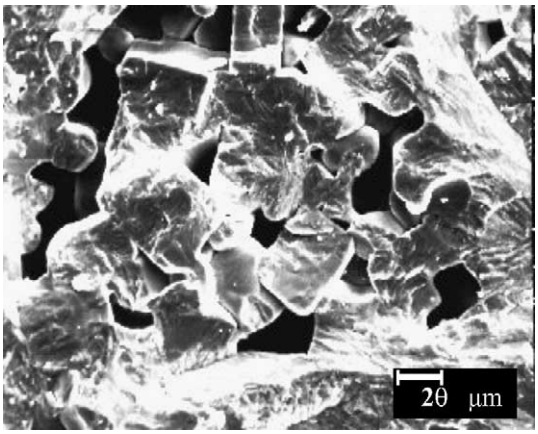

Fig. 1. SEM micrograph of the fracture surface of $Na_{0.80}K_{0.20}NbO_3$ sintered at 1100 °C for 2 h.

5 h to the complete burned out of the binder. The sintering was performed in air atmosphere at 1100 °C during 2 h. A 10 °C/min heating rate was used, while the cooling rate was fixed by the thermal inertia of the furnace. A density of 97% of the theoretical density (4.51 g/cm^3) was reached.

2.5. Microstructure

The final microstructure of $Na_{0.80}K_{0.20}NbO_3$ sintered at 1100 °C for 2 h in air atmosphere is shown in Fig. 1. The micrograph was taken on the fracture surface. The microstructure consists mainly of extensive sintered regions. Large voids can be identified being due to the grain pulled out during fracture process. Throughout careful visual inspection small solid regions or grain can be distinguished. The fracture mode is essentially intragranular being the grains with qualitative average size at around 40 μm. Based on the large number pulled grains during fracture process, we can expect that some part of fracture mode might exhibits a intergranular component. Furthermore, there is a slight residual porosity, which is in essence of intergranular nature.

2.6. Electrical characterization

Platinum electrodes were deposited on both faces of the sample by a platinum paste coating (Demetron 308A), which was dried at 800 °C during 30 min. The electrical measurements were performed in the frequency range 5 Hz–13 MHz, using a Hewlett-Packard HP 4192A impedance analyzer controlled by a personal computer. A 500 mV ac signal was applied. The samples were placed in a sample holder with a two-electrode configuration. The ac measurements were taken in several stages from room temperature to 800 °C in 50 °C steps. The temperature of measurement was held for 1 h prior to each measure. All the measurements were carried out in a dry air flow.

The impedance data ($Z^*(\omega)$) were plotted in the complex plane, a representation based on the plot of the real component ($Z'(\omega)$) vs. the imaginary component ($Z''(\omega)$). $Z^*(\omega)$ is represented by the equation $Z^*(\omega) = Z'(\omega) + jZ''(\omega)$. The data were normalized by the geometric factor S/l being S the area and l the thickness of ceramic sample, respectively. This procedure leads to an alternative and unequivocal representation of the impedance data, i.e., $\rho^*(\omega)$, according to equation $\rho^*(\omega) = (S/l)Z^*(\omega) = \rho'(\omega) + j\rho''(\omega)$, where $\rho^*(\omega)$ is the complex resistivity, j is the imaginary operator $\sqrt{-1}$.

Despite of the normalization, the $\rho'(\omega)$ against $\rho''(\omega)$ plot is typically termed as impedance diagram plot rather than the resistivity diagram plot. Theoretical fitting of the impedance data recorded at temperature above 400 °C was realized using software developed by Kleitz and Kennedy [13], which permits to determine some electrical parameters as resistance, capacitance and relaxation times with a precision better than 3%.

3. Results and discussion

3.1. Thermal analysis

Fig. 2 shows the thermal decomposition of the precursor. The overall weight loss was equal to 59% from room temperature to 900 °C. The TGA curve shows a 14% weight loss between 25 and 200 °C. In the same temperature range, the DTA curve shows two endothermic process positioned at around 83 and 139 °C, which are associated to the departure of water molecules during the thermal decomposition of the precursor (oxalato-niobium complex) [14]. According to TGA curve, the highest weight loss attain values at around 33%, occurring between 200 and 300 °C.

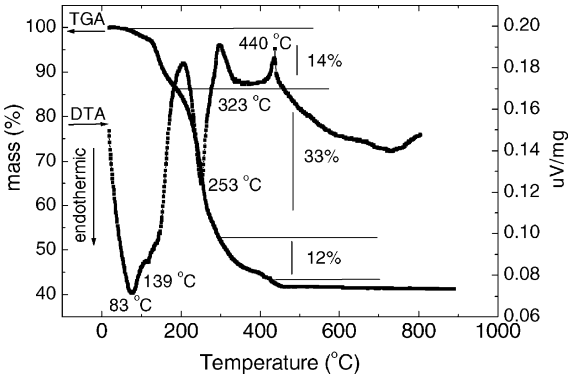

Fig. 2. TGA/DTA curves (10 °C/min) of $Na_{0.80}K_{0.20}NbO_3$ precursor powder.

These losses were correlated with the endothermic peak at 253 °C, in accordance with DTA curve. This endothermic process can be related to the elimination of water molecules, ammonium ions and CO and CO_2 molecules originated from the decomposition of an oxalate group. The elimination of these groups leads to the formation of an intermediate mono (oxalato) oxoniobate complex [10,11]. Between 300 and 400 °C, the TGA curve shows a weight loss of 12%, which can be assigned to the elimination of CO, from the mono(oxalato) complex decomposition. As a matter of fact, the thermal decomposition of simple or complex oxalates occurs with the formation of CO and CO_2, which can remain in the intermediate phase, adsorbed on the surface of the solid products [15]. The crystallization of the sodium potassium niobate was observed at 440 °C in the DTA curve. None weight loss and another thermal effect was observed above 450 °C indicating an absence of further decomposition above this temperature.

3.2. X-ray diffraction analysis

Fig. 3 shows the XRD pattern of $Na_{0.8}K_{0.20}NbO_3$ precursor powder calcined at 700 °C for 5 h. The $Na_{0.8}K_{0.20}NbO_3$ pattern is characteristic of the orthorhombic phase of $NaNbO_3$ [12]. However, a slight displacement of the 2θ position to higher values is observed with relation to the positions of $NaNbO_3$ (JCPDS card number 33-1270). Uncalcined precursor powder and calcined at 250 °C (data not shown here) exhibit an amorphous state. In this temperature range, the precursor powder is brownish. However, with the increase of the calcination temperature occurs an increasing of the crystallinity accomplished by increase of the diffraction peak intensities and a simultaneous decreasing in their breadths. The crystalline and single phase is obtained at 700 °C being of white color. The XRD results showed that during the course of the calcination, the formation of another crystalline phases does not occur. The lattice parameters of $Na_{0.80}K_{0.20}NbO_3$ powder were calculated via the least squares method. The results indicate an orthorhombic unit cell with lattice parameters: $a = 5.591$ Å, $b = 15.545$ Å, $c = 5.496$ Å.

3.3. Impedance analysis

The impedance diagrams for $Na_{0.80}K_{0.20}NbO_3$ ceramic presents a typical semicircle response [16,17],

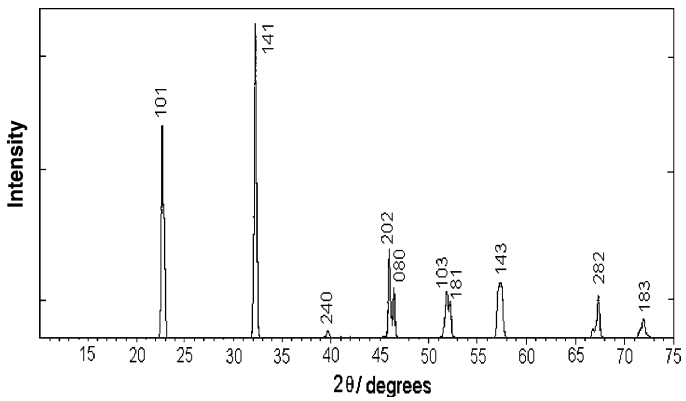

Fig. 3. XRD patterns of $Na_{0.80}K_{0.20}NbO_3$ precursor powder calcined at 700 °C for 5 h.

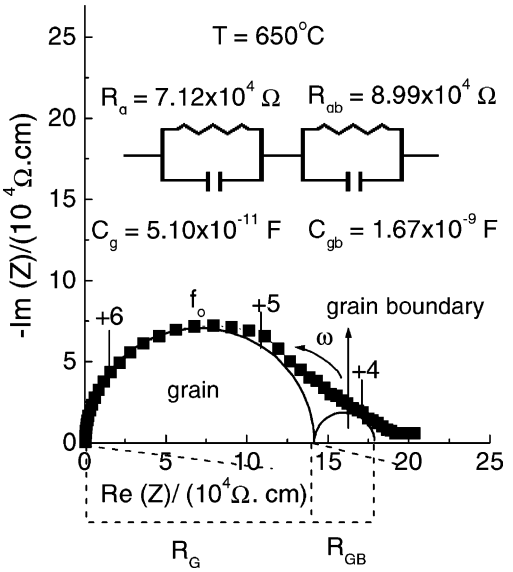

Fig. 4. Impedance diagram of $Na_{0.80}K_{0.20}NbO_3$ ceramic at 650 °C. Two parallel RC equivalent circuits are shown in the inset, corresponding to the electric and dielectric response of the solid solution. Numbers 4, 5 and 6 give the $\log_{10}$ (signal frequency) for the corresponding point.

as shown in Fig. 4. An equivalent electric circuit and its respective resistive and capacitive components were determined by theoretical adjustment, according to Section 2.6. The points on the diagram represent the experimental data, while the continuous line is the theoretical fitting. Both the electric and dielectric properties of the solid solution are further represented by two parallel RC equivalent circuits, as shown in the inset of Fig. 4. An excellent agreement between the experimental points and theoretical curve was attained. The first semicircle, in the high frequency range (>10 kHz), corresponds to an behavior of the intragranular of the material or bulk properties. The second semicircle represents the grain boundary contribution. This paper is exclusively focused on the bulk properties.

Fig. 5 shows $Z'(\omega)$ component as a function of frequency at different temperatures. Great variation on the resistance is observed between 350 and 400 °C (Fig. 5(a)) and 500 and 550 °C (Fig. 5(b)). Fig. 6 shows $Z''(\omega)$ component as a function of frequency, at several temperatures. The curves show broad and asymmetrical peaks, at around the frequency of maximum. Maximum and inflection points are observed.

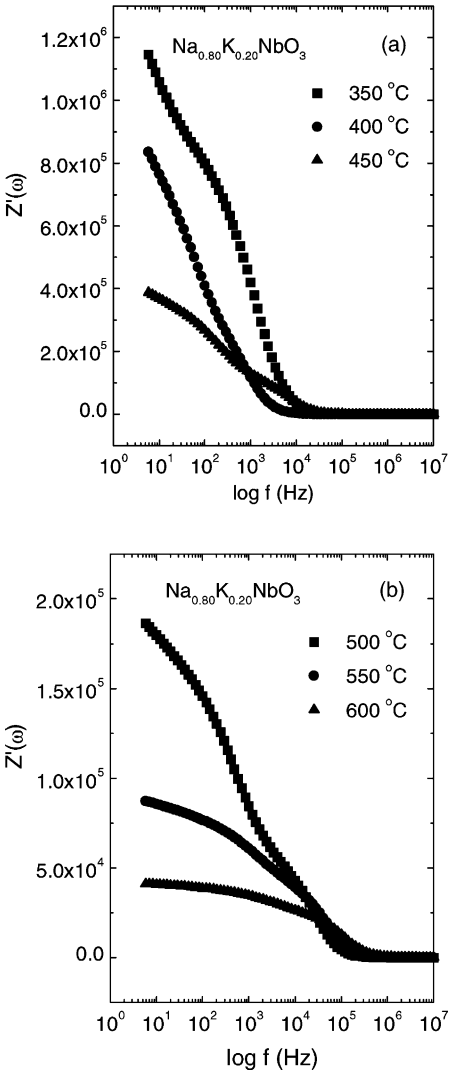

Fig. 5. Real part of impedance as a function of frequency at: (a) 350, 400, 450 °C and (b) 500, 550, 600 °C.

Both characteristic are a function of the temperature. In the temperature range investigated, two inflections are identified. The first inflection is shown at low frequency (0.1–1 kHz), while the second one is observed at around 10 kHz. However, at temperature ≥600 °C, only an unique inflection is apparent at high frequency region (≥10^2 kHz). According to Figs. 4–6, the first polarization phenomenon at low frequency is correlated to grain boundary contribution, while the second one is correlated to bulk or grain response. In addition,

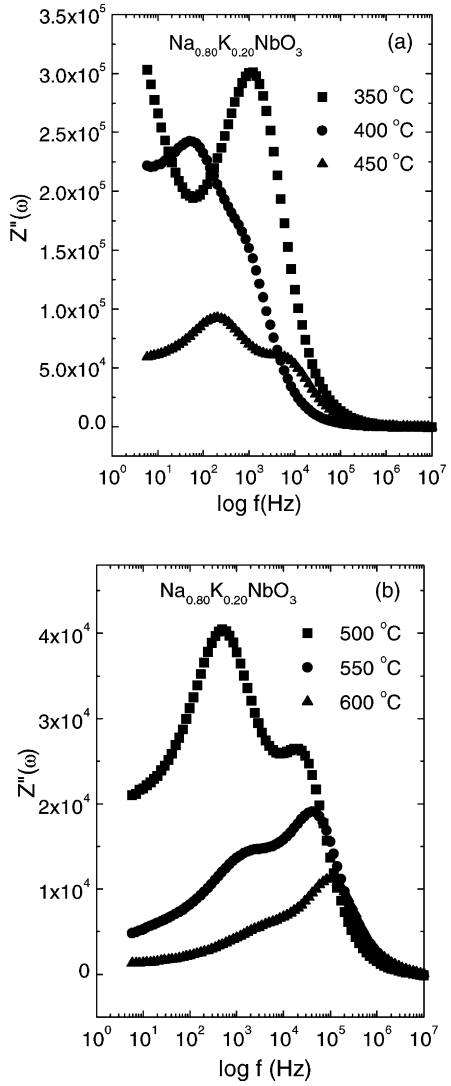

Fig. 6. Imaginary part of impedance as a function of frequency at: (a) 350, 400, 450 °C and (b) 500, 550, 600 °C.

the curve shapes suggest that there are two distributions of relaxation times with most frequent value at very similar frequency. Moreover, the frequency for the maximum f_0, relaxation frequency, shifts to higher values with increasing temperature.

3.4. Electric modulus analysis

An alternative approach to investigate the electrical response of a materials is to use the complex electrical modulus $M^*(\omega) = M'(\omega) + \mathrm{j}M''(\omega)$. This formalism is particularly suitable to detect phenomena as electrode polarization and bulk phenomenon property as average conductivity relaxation times τ_σ [18]. Complex modulus can be represented by the following equation:

$$M^*(\omega) = \frac{1}{\varepsilon^*(\omega)} = \mathrm{j}\omega C_0 Z^*(\omega) \quad (1)$$

where $\varepsilon^*(\omega)$ is the complex permittivity, $\mathrm{j} = \sqrt{-1}$ and C_0 is the vacuum capacitance of the cell.

Fig. 7(a) and (b) shows real part $M'(\omega)$ and imaginary parts $M''(\omega)$ of the electric modulus as a function of frequency logarithmic for $Na_{0.80}K_{0.20}NbO_3$ at several temperatures, respectively. According to Fig. 7(a), at all temperature investigated, $M'(\omega)$ shows a maximum at high frequency and it tends to zero at low frequencies suggesting negligible or absent of electrode polarization phenomenon [18]. The $M''(\omega)$ parameter shows a slightly asymmetric peak at each temperature, as can be see in Fig. 7(b). The peaks frequencies f_p shift to higher frequencies region with increasing temperature. Considering the parameter $M''(\omega)$, a shift in f_p suggest a variation of resistance. On the other hand, changes in the values of the maximum in $M''(\omega)$ with no variation in f_p suggest a change of resistance and capacitance [19]. However, Fig. 7(b) shows variations in both parameters magnitude and f_p of $M''(\omega)$ that indicate a variation of capacitance. Nevertheless, the combined representation of impedance and modulus spectroscopy permits to visualize better these phenomena. In $Z''(\omega)$ representation, a polarization phenomenon is highlighted with the largest resistance, whereas $M''(\omega)$ representation permits to observe those of the smallest capacitance. In $Z''(\omega)$ (Fig. 6) and $M''(\omega)$ (Fig. 7(b)) curves, the asymmetric development of both parameters provide additional evidence of two polarization phenomena, as mentioned previously. These polarization can be correlated to the grain and grain boundary contributions. Furthermore, both $Z''(\omega)$ and $M''(\omega)$ curves show at high frequency region (>10^5 Hz) an overlapping in all temperature range investigated being characteristic of long-range conductivity process [19]. As expected, this effect is accompanied by an increase of the $\tan\delta$ at low frequencies, as shown in Fig. 10.

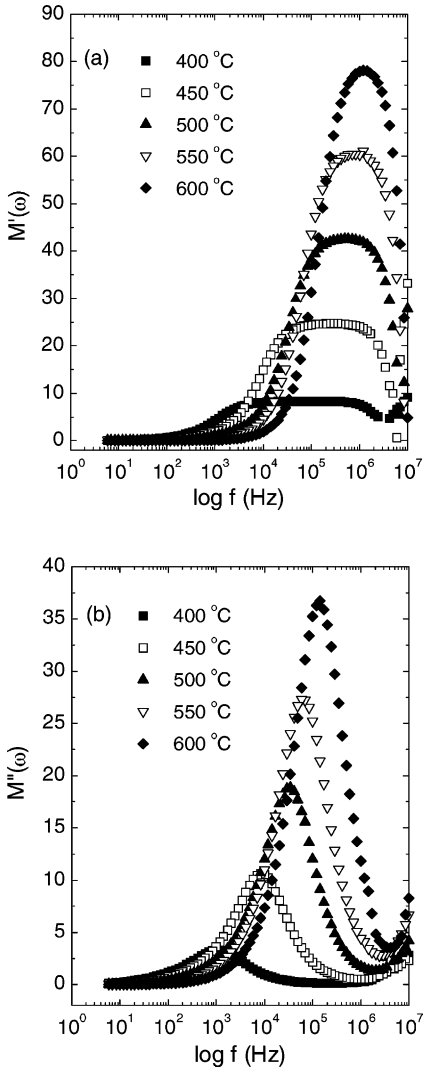

Fig. 7. (a) Real part of the electric modulus $M'(\omega)$ and (b) imaginary part of the electric modulus $M''(\omega)$ as a function of frequency logarithmic at several temperatures.

3.5. Dielectric behavior

Considering an ideal case, the impedance diagram is represented by Debye's expression, where the electrical response is simulated by a parallel circuit with a resistor (R) and an ideal capacitor (C), where $\omega_0 = 1/RC$ is the characteristic frequency of the equivalent circuit.

When, the data representation is given in the impedance diagram plot, the curve exhibits commonly a semicircular shape [20]. In high frequency regions, the diagram gives typically information on the bulk properties of the electroceramics. The semicircle diameter from the intercept with the real axis corresponds to the bulk resistance contribution (R). Thus, the bulk capacitance, C_b, called geometric capacitance can be derived from the relaxation time (τ) determined by relaxation:

$$\omega\tau = 1 \tag{2}$$

where ω is the angular frequency ($2\pi f$). The relaxation time can be alternatively derived by the equation $\tau = RC$, where R is the resistance and C the capacitance.

However, a non-ideal situation is typically observed. The Debye's expression is modified by introduction of an n factor. This modification leads to the Cole–Cole empirical behavior [21] described by the following equation:

$$Z^* = \frac{R}{1 + (\mathrm{j}\omega/\omega_0)^{1-n}} \tag{3}$$

The equation above shows that the center of the semicircle obtained by data plotting in the complex plane is located below of the real axis. Sometimes, the sample displays high resistivity behavior as occurs normally at low temperature and/or at room temperature. In this case, a typical theoretical fitting process is inadequate, since it leads to a gross error. Thus, an alternative approach to derive the dielectric permittivity [22] can be used considering the electrical response in the high frequency range using the following equation:

$$-\mathrm{Im}(Z) = \frac{1}{\mathrm{j}C_b 2\pi f} \tag{4}$$

where $-\mathrm{Im}(Z)$ is the opposite of the $Z''(\omega)$, j is the operator $\sqrt{-1}$.

Based on Eq. (4), the capacitance C_b of the sample is given by the slope of the straight line determined by the variation of $-\mathrm{Im}(Z)$ as a function of $1/2\pi f$. Since, the C_b parameter was determined, the permittivity, ε, can be derived by the equation $\varepsilon = C_b l/\varepsilon_0 S$, where ε_0 is the vacuum permittivity.

Fig. 8 shows the evolution of the permittivity of $Na_{0.80}K_{0.20}NbO_3$ solid solution as a function of temperature. Two maxima were observed. The maxima in the permittivity vs. temperature curves for $NaNbO_3$ [23] and $Na_{1-x}K_xNbO_3$ [5] have been ascribed to phase transitions. According to Francombe

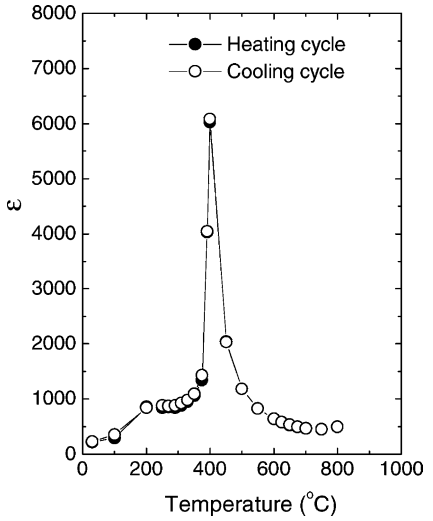

Fig. 8. Permittivity as a function of temperature for one thermal cycle.

and Lewis [6], $Na_{1-x}K_xNbO_3$ system is ferroelectric for $x > 0.1$. Below this value the coercitivity appears to be very large, while ferroelectric behavior cannot be observed. Curie's temperature (T_C) for $NaNbO_3$ determine the temperature of transition between a non-polar paraelectric state and an antiferroelectric state. However, The T_C in potassium sodium niobate corresponds to the ferroelectric–paraelectric transition. Furthermore, the sodium potassium niobate, where the coordination sites A are occupied by sodium and potassium, which present atomic radii equal to 0.98 and 1.38 Å, respectively, Curie's temperature increases from 360 to 400 °C. This suggests that the electronic configuration may be a significant property in the value of Curie's temperature. This may be effective through a change of polarizability. Thus, according to Fig. 8, the first maximum in the shoulder form positioned at very similar to 200 °C can be associated with an orthorhombic–tetragonal phase transition, while the second one positioned at around 400 °C, well-defined and of high intensity is assigned to the tetragonal–cubic phase transition. The dielectric permittivity curve of undoped $NaNbO_3$ ceramics during the heating step shows a maximum at 360 °C equal to 1000 [24]. This maximum is attributed to the tetragonal–cubic phase transition, which is correlated to the material Curie's temperature [6,23]. Thus, in $Na_{0.80}K_{0.20}NbO_3$ ceramic the maximum at 400 °C can be associated with Curie's temperature. However, in this system, Curie's temperature is characterized by tetragonal–cubic phase transition [5]. In this paper, at this temperature, the permittivity value is equal to 6000.

Considering $Na_{1-x}K_xNbO_3$ system, Curie's temperature rises with potassium concentration. Then, the temperature of the tetragonal–cubic phase transition shifts to below of Curie's temperature [6]. It is interesting to note that $Na_{0.80}K_{0.20}NbO_3$ solid solution does not exhibit significant thermal hysteresis on the permittivity curve during the heating and cooling steps. As a matter of fact, a very slight hysteresis is observed at temperature below the maximum permittivity indicating that the transition is not a pure first-order phase transition.

The dielectric constant ε can be expressed by complex permittivity in conventional way being $\varepsilon^*(\omega) = \varepsilon'(\omega) - j\varepsilon''(\omega)$, where $\varepsilon'(\omega)$ and $\varepsilon''(\omega)$ are the real and imaginary parts of the dielectric constant. Both parameters $\varepsilon'(\omega)$ and $\varepsilon''(\omega)$ can be extracted from impedance in a conventional way, according to the following equations:

$$\varepsilon'(w) = \frac{Z''}{2\pi f \varepsilon_0 G_f |Z|^2} \quad (5)$$

$$\varepsilon''(\omega) = \frac{Z'}{2\pi f \varepsilon_0 G_f |Z|^2} \quad (6)$$

where G_f is the geometric factor given by relation S/l (S the electrode area and l the sample thickness) and $|Z|^2$ is the impedance modulus. These equations have been previously reported [25]. However, some mechanics deficiencies has altered both $\varepsilon'(\omega)$ and $\varepsilon''(\omega)$ parameters representation [25]. By completeness, the data in Ref. [25] were adequately derived, according to Eqs. (5) and (6).

Fig. 9 shows the evolution of the $\varepsilon'(\omega)$ and $\varepsilon''(\omega)$ parameters as a function of frequency. Fig. 9(a) shows a log–log plot of $\varepsilon'(\omega)$ as a function of frequency, at several temperatures. A high degree of dispersion of the permittivity is identified at low frequencies ($<10^2$ kHz) with increasing temperature. In general, this behavior is found for dielectric materials, in which a mechanism conduction of the hopping type is present [26].

Depending on the temperature, the degree of the dispersion decreases with frequencies up to 10^2 kHz,

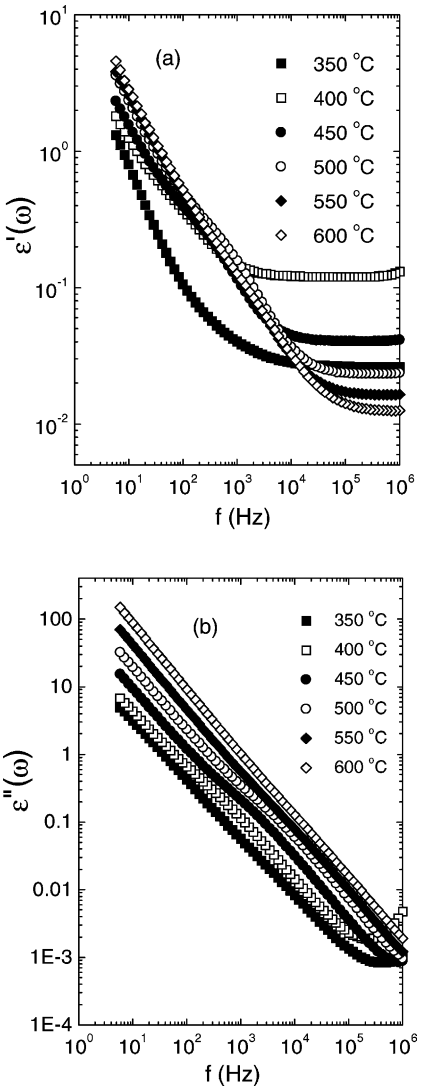

Fig. 9. Evolution of the complex permittivity as a function of frequency and temperature: (a) real part and (b) imaginary part.

between 10^2 and 10^3 kHz non-frequency dependence was observed. The plot of the $\varepsilon''(\omega)$ as a function of the frequency for $Na_{0.80}K_{0.20}NbO_3$ is shown in Fig. 9(b). The parameter $\varepsilon''(\omega)$ decreases with increasing frequency.

Fig. 10 shows the tangent losses, $\tan\delta = \varepsilon''(\omega)/\varepsilon'(\omega)$, as a function of temperature for frequencies of 1, 10, and 100 kHz and of 1 MHz. All the curves show a similar behavior at temperature below 500 °C. However, at temperatures above 500 °C, an

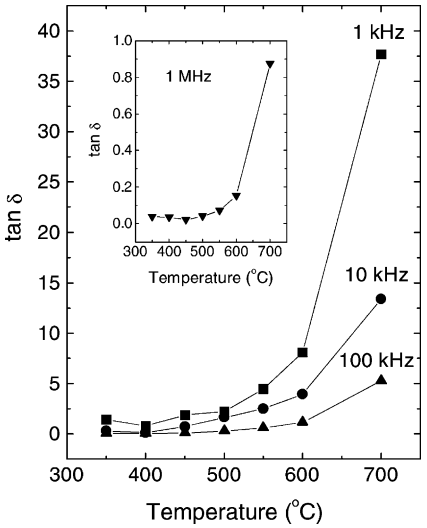

Fig. 10. $\tan\delta$ as a function of temperature for several frequencies of measurement.

intense increase of dielectric loss was observed for all frequencies of measurement. Generally speaking, the losses at high frequencies are much lower than those occurring at low frequencies. This kind of dependence of the $\tan\delta$ losses on frequency is typically associated with losses by conduction. Thus, at the measured permittivity value and owing to its low losses at high frequencies, the $Na_{0.80}K_{0.20}NbO_3$ solid solution demonstrates a potential for applications at high temperatures and microwave frequencies.

4. Conclusion

Stoichiometric, single phase and fine powder of $Na_{0.80}K_{0.20}NbO_3$ was obtained by chemical route using the evaporation solution method. An alternative approach applied to the dielectric characterization of $Na_{0.80}K_{0.20}NbO_3$, based on the geometric capacitance deriving, allowed the determination of the bulk permittivity with a high precision. The true dielectric permittivity is determined being eliminated any eventual contribution of the dc conduction process within the ceramic matrix that represents a strong advantage over fixed-frequency measurements. None of the significant thermal hysteresis was detected during the heating and cooling steps in the permittivity curve being

a further evidence of low susceptibility of dielectrical behavior with thermal processing.

Acknowledgements

The authors acknowledge CBMM (Companhia Brasileira de Metalurgia e Mineração, Araxá—MG, Brazil) for providing the niobium salt and Brazilian research funding institutions FAPESP, CNPq and CAPES.

References

[1] L. Egerton, D.M. Dillon, J. Am. Ceram. Soc. 42 (9) (1959) 438.
[2] R.E. Jaeger, L. Egerton, J. Am. Ceram. Soc. 45 (5) (1962) 209.
[3] H.D. Megaw, Ferroelectrics 7 (1974) 87.
[4] A. Reisman, F. Holtzberg, S. Triebwasser, M. Berkenblit, J. Am. Ceram. Soc. 78 (1956) 719.
[5] G. Shirane, R. Newnham, R. Pepinsky, Phys. Rev. 96 (3) (1954) 581.
[6] M.H. Francombe, B. Lewis, J. Electron. 2 (1957) 387.
[7] B.T. Mathias, J. Remeika, Phys. Ver. 82 (1951) 727.
[8] M.A.L. Nobre, S. Lanfredi, Mater. Lett. 50 (2001) 322.
[9] S. Lanfredi, P.S. Saia, R. Lebullenger, A.C. Hernandes, Solid State Ionic 146 (2002) 329.
[10] S. Lanfredi, L. Dessemond, A.C.M. Rodrigues, J. Eur. Ceram. Soc. 20 (2000) 983.
[11] S. Lanfredi, S. Folgueras-Domínguez, A.C.M. Rodrigues, J. Mater. Chem. 5 (11) (1995) 1957.
[12] Powder Diffraction File, Card No. 33–1270, Joint Committee on Powder Diffraction Standards, Swarthmore, PA.
[13] M. Kleitz, J.H. Kennedy, in: J. Mundy, G.P. Shenoy (Eds.), Fast Ion Transport in Solids, Elsevier, North-Holland, 1979, p. 185.
[14] M. Muller, J. Dehand, Bull. Soc. Chim. Fr. 8 (1971) 2837.
[15] L. Marta, M. Zaharescu, C.Gh. Macarovici, Rev. Roumaine Chim. 24 (8) (1979) 1115.
[16] M.A.L. Nobre, S. Lanfredi, J. Phys. Chem. Solids 62 (2001) 1999.
[17] S. Lanfredi, A.C.M. Rodrigues, J. Appl. Phys. 86 (4) (1999) 2215.
[18] R. Gerhardt, J. Phys. Chem. Solids 55 (12) (1994) 1491.
[19] A.R. James, S. Priya, K. Uchino, K. Srinivas, J. Appl. Phys. 90 (97) (2001) 3504.
[20] J.E. Bauerle, J. Phys. Chem. Solids 30 (1969) 2657.
[21] K.S. Cole, R.H. Cole, J. Chem. Phys. 9 (1941) 341.
[22] M.A.L. Nobre, S. Lanfredi, J. Phys. 12 (2000) 7833.
[23] L.E. Cross, B.J. Nicholson, J. Phil. Mag. 46 (1955) 453.
[24] L. Pardo, P. Dirán-Martin, J.P. Mercurio, L. Nibou, B. Jiménez, J. Phys. Chem. Solids 58 (9) (1997) 1335.
[25] M.A.L. Nobre, S. Lanfredi, Mater. Lett. 47 (2001) 362.
[26] H. Khemakhem, M. Mnif, J. Ravez, A. Daoud, J. Phys. Soc. Jpn. 68 (1999) 1031.